

Simulation of an
Integrated Transition Radiation and
Tracking Detector
for the ATLAS Experiment
at the LHC

M. Sc. Thesis

Mattias Ellert
Uppsala University, Department of Technology

Uppsala 1995

Abstract

A simulation study of an integrated transition radiation and tracking detector (TRT) prototype has been conducted in order to develop a reliable simulation tool for the inner detector of the future ATLAS experiment at the LHC.

The prototype consists of straw proportional tubes with a diameter of 4 mm. Due to this limited spatial extension of the sensitive parts of the detector the usual energy loss simulation based on the Bethe Bloch formula with Landau fluctuations has proven to be inadequate. Instead an implementation of the photoadsorption ionization (PAI) model described in this thesis has been used, giving better agreement between data and simulation.

The TRT will also be used for particle identification by the production and detection of transition radiation (TR). Different types of TR sources have been investigated by simulation: regular stacks of foils and more irregular sources, where the thicknesses of the layers of source material and of the gaps in-between those layers are varying, like in e.g. plastic foams.

The simulations show that small or moderate irregularities do not affect the total TR yield significantly and that foams therefore can be used with good results if they are not too irregular.

Contents

1	Introduction	3
1.1	The Large Hadron Collider (LHC)	3
1.2	The ATLAS Detector	4
1.3	The Inner Detector and the TRT	5
1.4	The RD6 Prototype, Experimental Setup	6
2	Particle Tracking and dE/dx Simulation	8
2.1	Tracking of Particles	8
2.2	Theory for the Energy Loss Simulation	8
2.3	Results of the Simulations	10
3	Transition Radiation	13
3.1	Theory for Transition Radiation	13
3.2	Detection of Transition Radiation	16
3.3	Results of the Simulations	16
4	Conclusions	22

Chapter 1

Introduction

1.1 The Large Hadron Collider (LHC)

The next particle collider project to be realized at CERN is the Large Hadron Collider (LHC). This is a proton proton collider which is to be built in the already existing 27 km tunnel used by the present Large Electron Positron Collider (LEP).

By using protons, almost 1000 times heavier than electrons, the particles can be accelerated to higher energies without experiencing the extensive radiative energy losses that are the case for relativistic electrons. The LHC is designed to accelerate protons to an energy of 7 TeV, giving a centre of mass energy of 14 TeV in a head on collision. This could be compared to the centre of mass energy of LEP, which is approx. 90 GeV.

Unlike electrons, protons have an internal structure of quarks and gluons. This makes the analysis of the collision events difficult. The ideal process would be to collide two quarks and see what happens, but this is impossible due to the quark confinement. Quarks possess colour charges and only objects with no total colour charge, like mesons (quark antiquark bound states) or baryons (three quark bound states), can exist in nature due to the vacuum opacity to colour, except during very short time intervals.

A proton is a baryon consisting of two up quarks and one down quark. Aside from these so called valence quarks the proton also consists of other constituents (partons). These are the gluons (strong force carriers holding the quarks together) and the sea quarks (quark antiquark pairs of all flavours constantly being created and annihilating with each other). The momentum of the proton is distributed among its constituents. On average a valence quark carries one sixth of the total momentum of the proton.

In “hard” collisions one constituent in one of the protons hits head on one constituent in the other proton. Due to the above mentioned distribution of momentum between the proton constituents the centre of mass energy in a collision between two valence quarks is on average only one sixth of the design energy of

the proton proton collider. This is still a significant increase from present colliders like LEP.

The statistical nature of the momentum distribution of the constituents imposes other problems on the experiments. When two leptons of equal momentum are collided, like in LEP today, the total momentum in the laboratory frame of reference is zero. On the other hand, when colliding two protons the two colliding constituents will in general not have equal momentum, making the total momentum non-zero in the laboratory frame.

The physical processes that will be studied at LHC have in general very low cross-sections. In order to obtain sufficient statistics many events must be studied in which these processes occur. This imposes a requirement of high luminosity on the collider and the LHC is designed for a luminosity of $10^{34} \text{ cm}^{-2}\text{s}^{-1}$ requiring a bunch spacing of 25 ns and 10^{11} particles in each bunch. In each bunch crossing several collisions take place, but very few are “hard” head on collisions between two proton constituents. For each such event there will be several minimum bias events. This too imposes strong requirements on the detectors. The short bunch spacing (25 ns) also implies that the detectors have to be very fast.

Centre of mass energy	14.0 TeV
Dipole field	8.65 T
Luminosity	$10^{34} \text{ cm}^{-2}\text{s}^{-1}$
Bunch spacing	25 ns
Particles per bunch	10^{11}
Stored beam energy	332 MJ
Bunch length (r.m.s.)	0.075 m
Crossing angle	200 μrad
Beam lifetime	22 h
Energy loss per turn	6.9 keV

Table 1.1: Design parameters for the Large Hadron Collider (LHC)

1.2 The ATLAS Detector

Two general purpose experiments are planned for the LHC — ATLAS and CMS. These are complex detector systems each consisting of many different subdetectors. The ATLAS detector is a large construction, the overall dimensions are a cylinder of length 30 m and diameter 20 m. The different subdetectors are more or less the same as those that can be found in a present LEP experiment: an inner detector, an electromagnetic calorimeter, a hadronic calorimeter and muon chambers. The main differences are that the sizes are larger at LHC, the demands

imposed on the detectors by the high complexity of the events and the need for fast triggering and electronic read-out. A description of the different parts of the detector can be found in the Technical Proposal [1].

The ATLAS detector is called a general purpose detector because it is designed to be used in several different types of physics research. One of the main purposes of the detector is the search for the Higgs boson which is responsible for the non-zero mass of the W^\pm and Z^0 gauge bosons of the weak interaction in the standard model. Other topics that will be explored with the ATLAS detector are precise measurements of the top quark mass and research on CP-violation in B-meson decays.

In order to optimize the design of the different subdetectors, extensive Monte Carlo simulations of events and of the response of the detectors to those events have to be done. To obtain reliability for those simulations different prototypes of the subdetectors have been built and the aim is to tune the simulation software so that it reproduces the results obtained by the different prototypes.

1.3 The Inner Detector and the TRT

This thesis is about the integrated transition radiation and tracking detector (TRT) that is part of the inner detector in the ATLAS experiment.

The TRT has two major purposes, as is indicated by its name. The first is to supply a means for particle identification by the production and detection of transition radiation (TR) [2]. This electromagnetic radiation is produced when a charged particle passes a boundary between two media with different dielectric properties. For each particle there exists a cut-off energy above which the intensity of the emitted TR spectrum falls rapidly. This cut-off energy is proportional to the Lorentz γ -factor of the particle. This means that for very relativistic particles, like high energy electrons, the transition radiation spectrum extends into the X-ray region, while for slower particles, like pions of the same energy, the spectrum is limited to the visible or ultraviolet regions. By making the detector sensitive to X-ray photons an electron pion separation is obtained.

The second purpose of the TRT is to track charged particles through the inner detector [3]. These two functions have been integrated by letting the same detector detect both the TR photons and the ionizations caused by the charged particles traversing the detector. The tracking ability of the inner detector is further improved by a few high precision measurements with semiconductor trackers (SCT) and/or microstrip gas counters (MSGC) on each track.

The TRT has good radiation hardness. Experiments have shown that the straws work without any degradation in performance after the radiation dose that will be accumulated during 10 years of LHC running. This gives robustness to the design since the TRT alone can be used for tracking (with a somewhat worse resolution) even in case the semiconductor trackers would fail due to irra-

diation. The inner detector is also important for the level-2 trigger of the ATLAS experiment [4].

1.4 The RD6 Prototype, Experimental Setup

The development of an integrated transition radiation and tracking detector (TRT) for the LHC began with the submission of a proposal to the Detector Research and Development Committee (DRDC) at CERN in August 1990 [5]. The project was approved by the Research Board under the name RD6. Since then several status reports of the project have been presented by the RD6 collaboration [6, 7]. At present the development of the TRT is continuing and it is now carried out with the joint efforts of the RD6 and ATLAS collaborations with the aim to integrate the TRT as a part of the inner detector of the ATLAS experiment.

During the development of the inner detector several prototypes have been built by the RD6 collaboration. In this thesis we will describe the so called second generation TRT prototype.

The prototype consists of straw proportional tubes [8] embedded in a polyethene foam with a density of 59 g/cm^3 . The purpose of the foam is to serve as a transition radiation source when it is traversed by relativistic particles. It also provides mechanical support and rigidity for the straws. The straws in the prototype are separated into four blocks each containing 24 rows of straws. The rows are separated by a distance of 8 mm as are the straws themselves within each row. The rows are placed with a random offset with respect to each other in order to obtain uniformity in the detector. In total the number of straws in the prototype is 864. See fig. 1.1 for a sketch of the prototype detector layout.

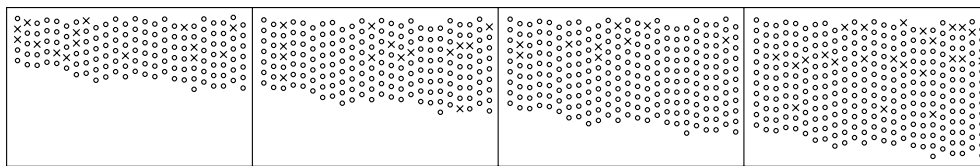


Figure 1.1: The layout of the straws in the RD6 prototype.

The 40 cm long straws have a diameter of 4 mm and are filled with a gas mixture of 70% xenon (Xe), 20% carbon dioxide (CO_2) and 10% tetrafluoromethane (CF_4). This mixture combines several desirable properties like short drift time (CF_4), stability against discharges (CO_2), and efficient absorption of transition radiation (Xe).

The prototype was tested using a beam from the SPS at CERN during July to September 1991 and June to July 1992. The straws were operated at a gas

gain of approx. 10^4 . Despite the moderate gas gain the long drift time of positive ions in the straws gave rise to non-linear effects due to the accumulated space charge. These non-linearities were measured and included in the simulations.

The performance of the individual straws varied during the data acquisition. Some straws were very noisy and indicated hits at an abnormally high rate. Straws with a hit frequency higher than 40% were identified and defined as noisy. Other straws were dead and gave no signal at all. The noisy and the dead straws were flagged and excluded from the analysis. These straws were also excluded from the simulated events in order to obtain comparability. Altogether 7% of the straws were excluded. The excluded straws have been crossed out in fig. 1.1.

Chapter 2

Particle Tracking and dE/dx Simulation

2.1 Tracking of Particles

The tracking of the particles through the simulated detector was done by the GEANT detector simulation package (version 3.15) developed at CERN [9].

2.2 Theory for the Energy Loss Simulation

The traditional way to simulate the response of the sensitive parts of a detector is to simulate the energy loss, dE/dx , using the Bethe Bloch formula and imposing a Landau fluctuation on the result. The main drawback of this method is its incapacity of simulating the energy loss spectrum in “thin” detectors where the number of primary collisions is small and a method based on a continuous energy loss is inadequate.

An alternative way to simulate the energy loss is to use the photoadsorption ionization (PAI) model. This is a two step model. In the first step the primary ionizations along the track are simulated. The energy loss of the particle can be described by a Poisson process where the number of primary interactions in a given distance is given by a Poisson distribution. In a Poisson process the time between two subsequent events follows an exponential distribution. The distribution of the distances travelled by the particle between two primary interactions can then be written as

$$f(x) = \frac{e^{-x/\lambda}}{\lambda} , \quad (2.1)$$

where λ is the mean free path length of the particle in the medium. In order to obtain a random number from this distribution the following formula can be used:

$$x = -\lambda \log \xi , \quad (2.2)$$

where ξ is a random number from a uniform distribution between 0 and 1. This is the basis of the Monte Carlo implementation of the model.

In the second step the energy transfer in each of the primary collisions is simulated. For this purpose the differential distribution of the energy losses according to the PAI model was used [10]:

$$\begin{aligned} \frac{d^2N}{dE dx} = & -\frac{e^2}{\pi\hbar^2 c^2} \text{Im} \left[\left(\frac{1}{\beta^2 \varepsilon} - 1 \right) \log \frac{2m_e v^2}{E(1 - \beta^2 \varepsilon)} \right] \\ & + \frac{2\pi e^4 N_e}{m_e v^2 E^2} \int_0^E \frac{f(E')}{|\varepsilon(E')|^2} dE' , \end{aligned} \quad (2.3)$$

where N is the number of energy transfers, E the transferred energy, x is the distance travelled by the particle; e and m_e are the electron charge and mass respectively, \hbar is the reduced Planck's constant; c is the speed of light, v is the velocity of the particle and $\beta = v/c$. N_e is the electron density, $f(E)$ are the oscillator strengths as described below and ε is the complex dielectric constant given by [10]

$$\varepsilon(E) = 1 - E_{\text{pl}}^2 \int_0^\infty \frac{f(E') dE'}{E^2 - E'^2 + 2i\eta E} . \quad (2.4)$$

In this formula η is a parameter inserted to avoid singularities and is set to 1 eV in these calculations. The results are not very sensitive to the value of this parameter. E_{pl} is the plasma energy given by

$$E_{\text{pl}} = \sqrt{\frac{4\pi e^2 \hbar^2 N_e}{m_e}} . \quad (2.5)$$

The oscillator strengths, $f(E)$, are proportional to the photoabsorption cross-sections, σ_γ , in the following way [11, 12]:

$$f(E) = \frac{\sigma_\gamma(E)}{2\pi^2 \hbar c \frac{e^2}{m_e c^2} Z} , \quad (2.6)$$

where Z is the atomic number of the detector material. If the sensitive part of the detector consists of compounds or mixtures of different types of atoms average values should be used for the cross-sections and the atomic number:

$$f(E) = \frac{\sum_i w_i \sigma_{\gamma,i}(E)}{2\pi^2 \hbar c \frac{e^2}{m_e c^2} \sum_i w_i Z_i} , \quad (2.7)$$

where the weights, w_i , are proportional to the number of atoms of each element, i .

According to the Thomas Reich Kuhn sum rule the oscillator strengths satisfy the integral

$$\int_0^\infty f(E) dE = 1 . \quad (2.8)$$

This sum rule is only valid if the minimum ionizing potential of the material is zero. In other cases it is a few percent wrong and should not be used for renormalization of the oscillator strengths.

The mean total number of energy transfers in a given path length can be computed as

$$\frac{dN}{dx} = \int_{E_{\min}}^{\infty} \frac{d^2N}{dE dx} dE, \quad (2.9)$$

where E_{\min} is the minimum ionizing potential of the medium. From this the mean free path length used in equation (2.1) can easily be obtained:

$$\lambda = \frac{1}{\frac{dN}{dx}}. \quad (2.10)$$

2.3 Results of the Simulations

The simulations were performed on the IBM mainframe computer (CERNVM) at CERN using a program put together from routines in the ATLAS program library by Dr. Wolfgang Funk of the RD6 collaboration.

The response of the detector was studied for different particle beams. In this simulation study the response to two different beams was investigated: 20 GeV pions and 30 GeV electrons. The former has a very low transition radiation yield and is therefore suitable for studying the relevancy of the dE/dx simulation. In fig. 2.1 the energy spectrum of the straws on the fitted track is shown for the measured data as well as for the simulation.

As can be seen from fig. 2.1 the agreement between data and simulation is good, except for a discrepancy in the simulation for the lowest part of the energy spectrum. This spectrum is however significantly better than the spectrum obtained with the Bethe Bloch formula with Landau fluctuations (default option in GEANT), shown in fig. 2.2.

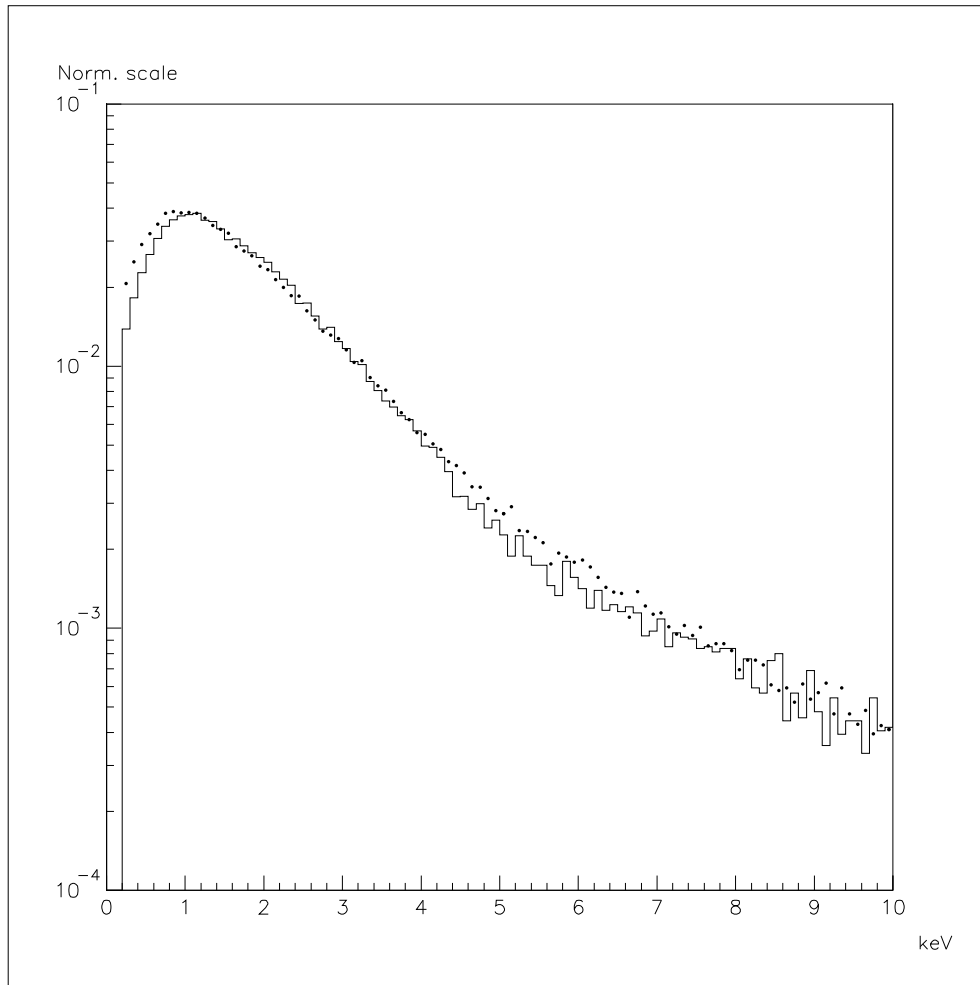


Figure 2.1: Energy spectrum of the hit straws (deposited energy larger than 200 eV) on the fitted track for 20 GeV pions. The solid line represents simulated events using the PAI model as described in this chapter. The dots represent measured data from the prototype.

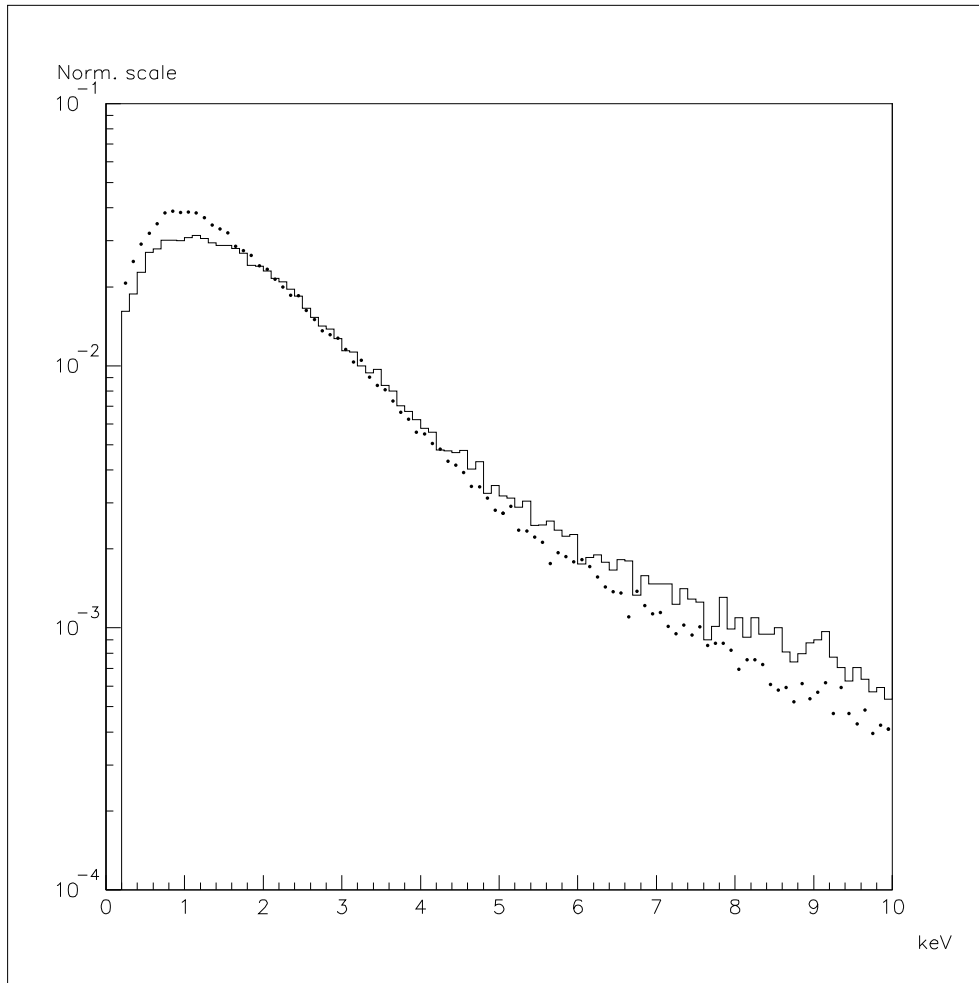


Figure 2.2: Same as fig. 2.1 except that the simulation was done using the Bethe Bloch formula with Landau fluctuations.

Chapter 3

Transition Radiation

3.1 Theory for Transition Radiation

Transition radiation (TR) is the electromagnetic radiation that is emitted when a charged particle traverses a boundary between two media with different dielectric properties. This radiation was predicted from Maxwell's equations by Ginzburg and Frank [13] in 1944 and later detected experimentally. However, the number of TR photons produced in a single transition between two media is small. By letting the particle pass through a material with many boundaries (hereafter called a radiator), e.g. a stack of foils (with air between each foil) or a plastic foam, the yield can be increased.

The value of the dielectric coefficient, ϵ_k , of a medium, k , depends on the energy, E , of the electromagnetic radiation. For each medium this dependence can be written as

$$\epsilon_k = 1 - \frac{E_k^2}{E^2}, \quad (3.1)$$

where E_k is the plasma energy of the medium. The plasma energy can be calculated from the electron density, $N_{e,k}$, (the number of electrons per unit volume) in the medium.

$$E_k = \sqrt{\frac{4\pi e^2 \hbar^2 N_{e,k}}{m_e}}, \quad (3.2)$$

where e and m_e are the electron charge and mass respectively and \hbar is the reduced Planck's constant.

The differential TR spectrum from a particle with unit charge traversing perpendicular through a boundary between two media with plasma energies E_1 and E_2 is given by the formula [14]

$$\frac{d^2 N_0}{dE d\theta} = \frac{2\alpha\theta^3}{\pi E} \left(\frac{1}{1/\gamma^2 + \theta^2 + E_1^2/E^2} - \frac{1}{1/\gamma^2 + \theta^2 + E_2^2/E^2} \right)^2, \quad (3.3)$$

where N_0 is the number of emitted TR photons, θ is the angle of emission with respect to the particle trajectory and γ is the Lorentz γ -factor. In this simple case the energy spectrum can be obtained by integration.

$$\begin{aligned} \frac{dN_0}{dE} &= \int_0^\pi \frac{d^2N_0}{dE d\theta} d\theta \\ &= \frac{\alpha}{\pi E} \left[\left(\frac{E_1^2 + E_2^2 + 2E^2/\gamma^2}{E_1^2 - E_2^2} \right) \log \left(\frac{1/\gamma^2 + E_1^2/E^2}{1/\gamma^2 + E_2^2/E^2} \right) - 2 \right] \end{aligned} \quad (3.4)$$

When the particle traverses several boundaries the calculation of the TR yield is not as easy. Due to interference effects the total yield is not equal to the sum of the yields from each single transition. In this case the differential spectrum is usually written as

$$\frac{d^2N}{dE d\theta} = \frac{d^2N_0}{dE d\theta} \cdot I, \quad (3.5)$$

where I has different forms in different cases. For a radiator consisting of a regular stack of N_f equal foils of thickness l_1 with equal spacing l_2 between each foil I is given by [14]

$$I = 4 \sin^2 \left(\frac{l_1}{Z_1} \right) \frac{\sin^2 [N_f (l_1/Z_1 + l_2/Z_2)]}{\sin^2 (l_1/Z_1 + l_2/Z_2)}, \quad (3.6)$$

where the so called formation zones Z_k are given by

$$Z_k = \frac{4\hbar c}{E} \left(\frac{1}{\gamma^2} + \theta^2 + \frac{E_k^2}{E^2} \right)^{-1}. \quad (3.7)$$

To obtain the energy spectrum for the regular stack equation (3.5), with the I given by equation (3.6) inserted, must be integrated over all angles. The result of this integration (for $E_1 > E_2$) is [14]:

$$\begin{aligned} \frac{dN}{dE} &= 2\alpha\hbar c N_f \frac{(E_1^2 - E_2^2)^2}{E^3} (l_1 + l_2)^2 \\ &\sum_n \left\{ \frac{2\pi\hbar c n - \frac{(l_1+l_2)E}{2\gamma^2} - \frac{l_1 E_1^2 + l_2 E_2^2}{2E}}{\left(\frac{l_1(E_1^2 - E_2^2)}{2E} - 2\pi\hbar c n \right)^2 \left(\frac{l_2(E_2^2 - E_1^2)}{2E} - 2\pi\hbar c n \right)^2} \right. \\ &\left. \sin^2 \left[\frac{l_2}{l_1 + l_2} \left(\frac{l_1}{4\hbar c E} (E_1^2 - E_2^2) - \pi n \right) \right] \right\}, \end{aligned} \quad (3.8)$$

where the sum is taken over all integers $n \in [n_{\min}, n_{\max}]$ for which the term in the braces is positive.

$$n_{\min} = \frac{l_1 + l_2}{2\pi\gamma\hbar c} \sqrt{\frac{l_1 E_1^2 + l_2 E_2^2}{l_1 + l_2}} \quad (3.9)$$

$$n_{\max} = \gamma n_{\min} \quad (3.10)$$

For an irregular stack, or a foam, these results do not apply. Instead the yield can be calculated by the following formula [15, 16], here adapted to the case $E_2 \neq 0$.

$$I = 2 \left[N_f \operatorname{Re} \left(\frac{Q}{W} \right) + \operatorname{Re} \left(\frac{U^2 h_2 V}{W^2} \right) \right], \quad (3.11)$$

where

$$Q = (1 - h_1)(1 - h_2) \quad (3.12)$$

$$W = 1 - h_1 h_2 \quad (3.13)$$

$$U = 1 - h_1 \quad (3.14)$$

$$V = 1 - h_1^N h_2^N \quad (3.15)$$

$$h_k = \langle e^{-i\phi_k l_k} \rangle \quad (3.16)$$

$$\phi_k = \frac{E}{\hbar v} - \frac{E}{\hbar c} \sqrt{\varepsilon_k - \sin^2 \theta} \quad (3.17)$$

and the $\langle \text{brackets} \rangle$ indicate the average of the enclosed expression taken over all foil thicknesses or gap spacings respectively, or, in the case of a foam, over the wall thicknesses and cell sizes respectively. In order to evaluate these averages the distribution of the material and gap thicknesses must be known.

In many cases the measured distributions are compatible with a Γ -distribution:

$$f(l_k) = \frac{\beta_k^{\alpha_k} l_k^{\alpha_k - 1} e^{-\beta_k l_k}}{\Gamma(\alpha_k)}, \quad (3.18)$$

where the parameters α_k and β_k are given by

$$\alpha_k = \frac{\langle l_k \rangle^2}{\langle \Delta l_k^2 \rangle} \quad (3.19)$$

$$\beta_k = \frac{\langle l_k \rangle}{\langle \Delta l_k^2 \rangle}, \quad (3.20)$$

where $\langle \Delta x^2 \rangle$ indicates the statistical variance of the distribution of the variable x . The parameters α_k and β_k are by this definition a measure of the irregularity of the radiator. A smaller value indicates a more irregular radiator, while a larger value corresponds to a more regular radiator. The regular stack of foils corresponds to a value of infinity. With this distribution

$$h_k = m_k e^{i\psi_k} \quad (3.21)$$

$$m_k = \left[1 + \left(\frac{\phi_k \langle l_k \rangle}{\alpha_k} \right)^2 \right]^{-\alpha_k/2} \quad (3.22)$$

$$\psi_k = -\alpha_k \arctan \frac{\phi_k \langle l_k \rangle}{\alpha_k}. \quad (3.23)$$

The energy spectrum can then be obtained by numerical integration of equation (3.5) with the I given by equation (3.11), into which the above results for the Γ -distribution case have been substituted.

3.2 Detection of Transition Radiation

In order to detect the transition radiation photons with high probability, the sensitive gas in the detector straws must have a high photoelectric cross-section. This is the reason for the choice of xenon as the main component in the gas mixture.

The use of transition radiation as a means for particle identification at relativistic energies is favoured over other methods by the linear dependence of the total TR energy loss on the Lorentz γ -factor (in the case of a single transition).

$$\Delta E = \int_0^\infty E \frac{dN_0}{dE} dE = \frac{\alpha (E_1 - E_2)^2}{3 (E_1 + E_2)} \gamma \quad (3.24)$$

When the particle passes several boundaries this dependence is not exact due to the interference effects, and the energy loss saturates at some γ . Nevertheless, transition radiation is still a good tool for particle identification at relativistic energies, and this is the main reason for the use of transition radiation detectors [17].

The TR spectrum is strongly peaked in the forward direction. This means that the TR photons are mainly emitted along the trajectory of the generating particle. Hence the straws in which the TR photons are detected are lying on the particle track.

3.3 Results of the Simulations

The same computer program was used for the simulations as before. Some additional lines of code were written to implement the calculation of the TR yield from irregular sources described earlier in this chapter.

In the following examples the calculations have been carried out for a particle with unit charge traversing 50 foils (or foam cell walls) with a Lorentz γ -factor of 58700, corresponding to a 30 GeV electron. The parameters used in the examples are $\langle l_1 \rangle = 13 \mu\text{m}$, $\langle l_2 \rangle = 195 \mu\text{m}$, $E_1 = 44.8 \text{ eV}$ and $E_2 = 0.73 \text{ eV}$, corresponding to the plastic foam used in the prototype.

Fig. 3.1 shows the angular distribution of TR photons with an energy of 4 keV from radiators with different degrees of irregularity. As can be seen from the graph, the spectrum changes more rapidly for more regular radiators. This is due to the interference effects. In the limit of a completely regular radiator the spectrum approaches what can be described as a sum of δ -functions, explaining

why in this case the integrated spectrum can be computed as a sum as in equation (3.8).

Fig. 3.2 shows the energy spectrum of the TR photons obtained by integrating over all angles. The graph also shows the spectrum for the regular case obtained from equation (3.8). Once again it can be seen that the spectrum for the regular case has several maxima and minima originating from interference effects. These effects average out more and more the more irregular the radiator becomes. For the most irregular cases, in addition to the absence of interference effects, a significant drop in the TR yield can be seen.

From a computational point of view it can be said that the regular case requires less computational effort since there is no need for numerical integration. On the other hand is the spectrum more varying in this case which makes it necessary to calculate more points in order to be able to make good interpolations.

A regular stack of foils has a larger TR yield than an irregular stack or a foam. A more regular foam like polyethene has a higher yield than a more irregular foam like polystyrene (see fig. 3.3). This is the reason for using polyethene as radiator in the prototype. The reason for using a foam instead of foils is that a foam can provide mechanical support and rigidity to the straws.

The simulation of the TR spectrum can be compared to the spectrum measured for the 30 GeV electron beam. The result can be seen in fig. 3.4. As can be seen the simulation is in fair agreement with the data.

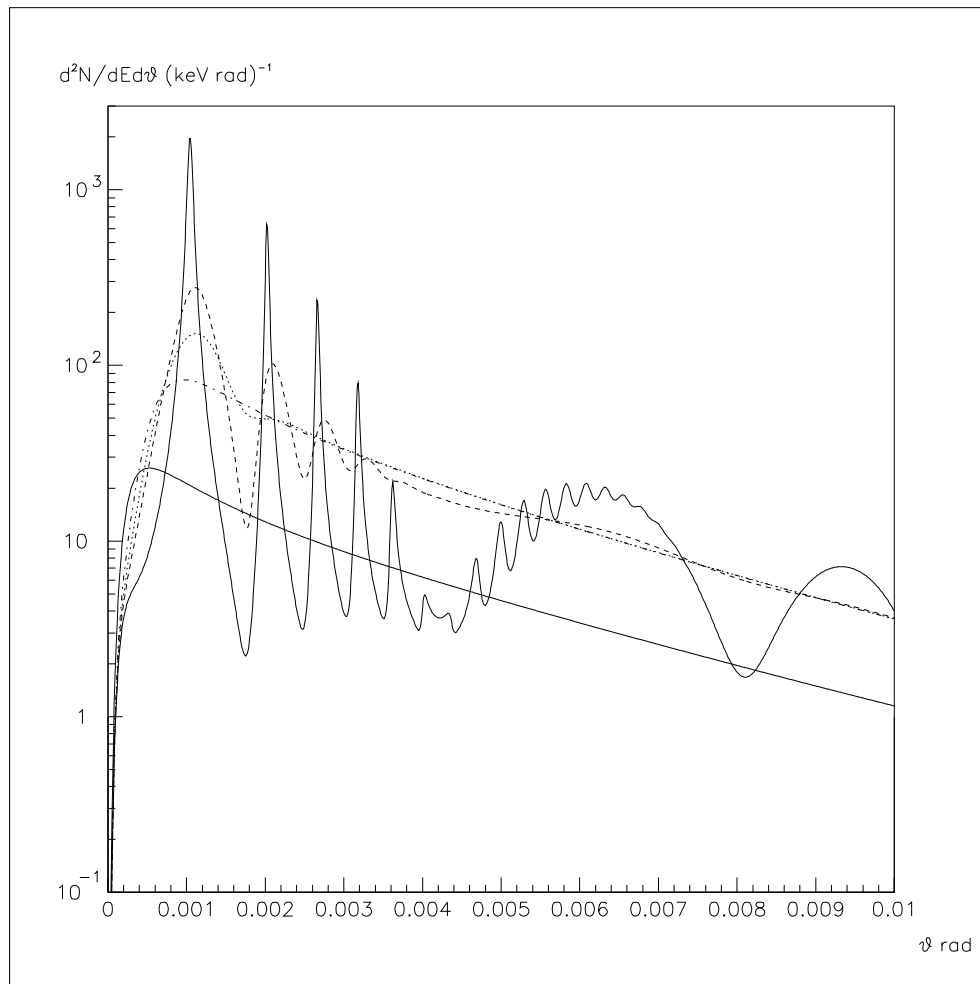


Figure 3.1: Angular distribution of 4 keV transition radiation photons from a particle with $\gamma = 58700$ traversing 50 foils or foam cell walls. The parameters used when calculating the graphs are $\langle l_1 \rangle = 13 \mu\text{m}$, $\langle l_2 \rangle = 195 \mu\text{m}$, $E_1 = 44.8 \text{ eV}$ and $E_2 = 0.73 \text{ eV}$. The different graphs correspond to different irregularities: $\alpha_1 = \alpha_2 = 1000$ (fast varying solid line), 100 (dashed line), 10 (dotted line), 1 (dash-dotted line) and 0.1 (smooth solid line).

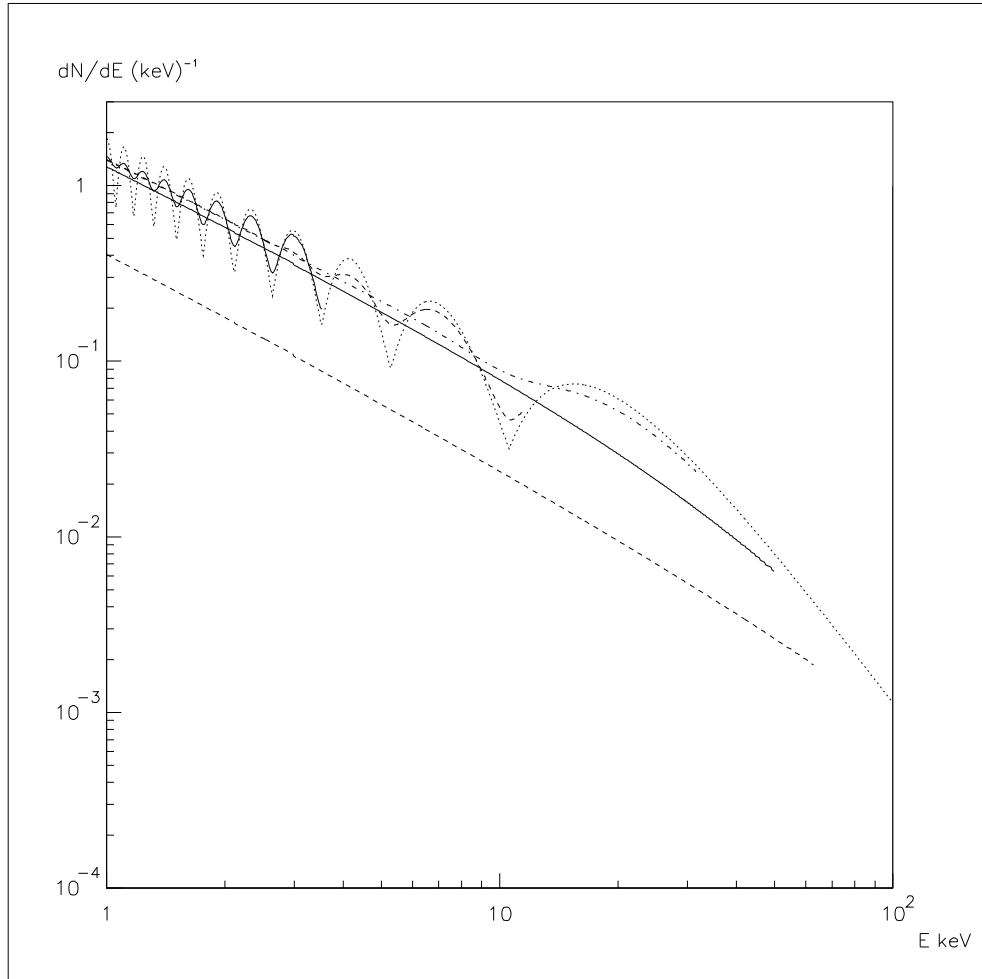


Figure 3.2: Energy spectrum of the transition radiation photons caused by a particle with $\gamma = 58700$ traversing a radiator consisting of 50 foils or foam cell walls. The parameters used when calculating the graphs are the same as in fig. 3.1. The different graphs correspond to the regular case (dotted line) and different irregular cases: $\alpha_1 = \alpha_2 = 1000$ (fast varying solid line), 100 (varying dashed line), 10 (dash-dotted line), 1 (smooth solid line) and 0.1 (smooth dashed line).

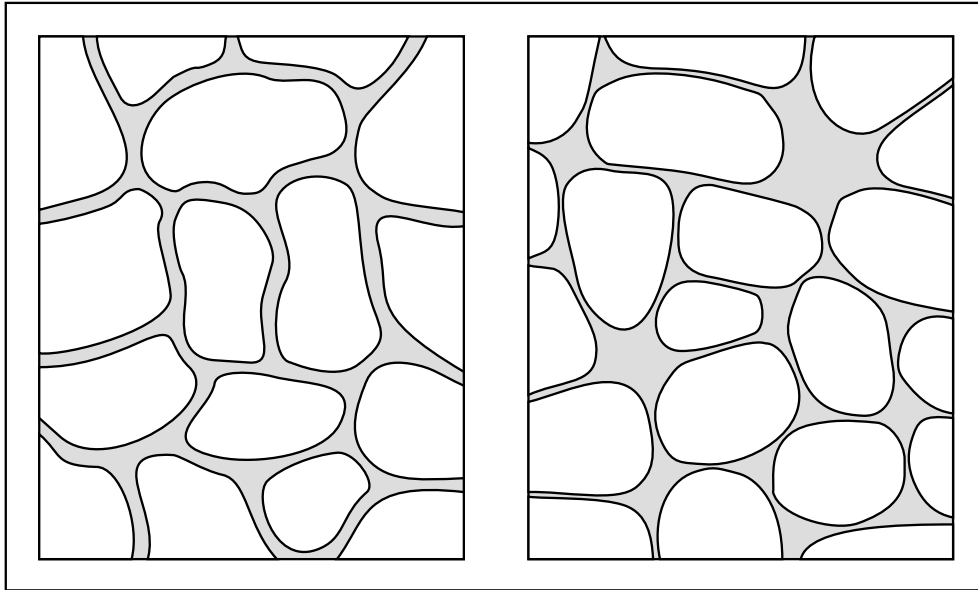


Figure 3.3: Structures of different plastic foams. To the left a foam with regular wall thicknesses between the cells is shown. This is very similar to the structure of the polyethylene foam used in the prototype. To the right a more irregular foam is shown, similar to the structure of a polystyrene foam. In this foam the walls between the cells are very thin and most of the plastic material is located in lumps between the cells. The more regular foam to the left gives a higher TR yield than the more irregular to the right.

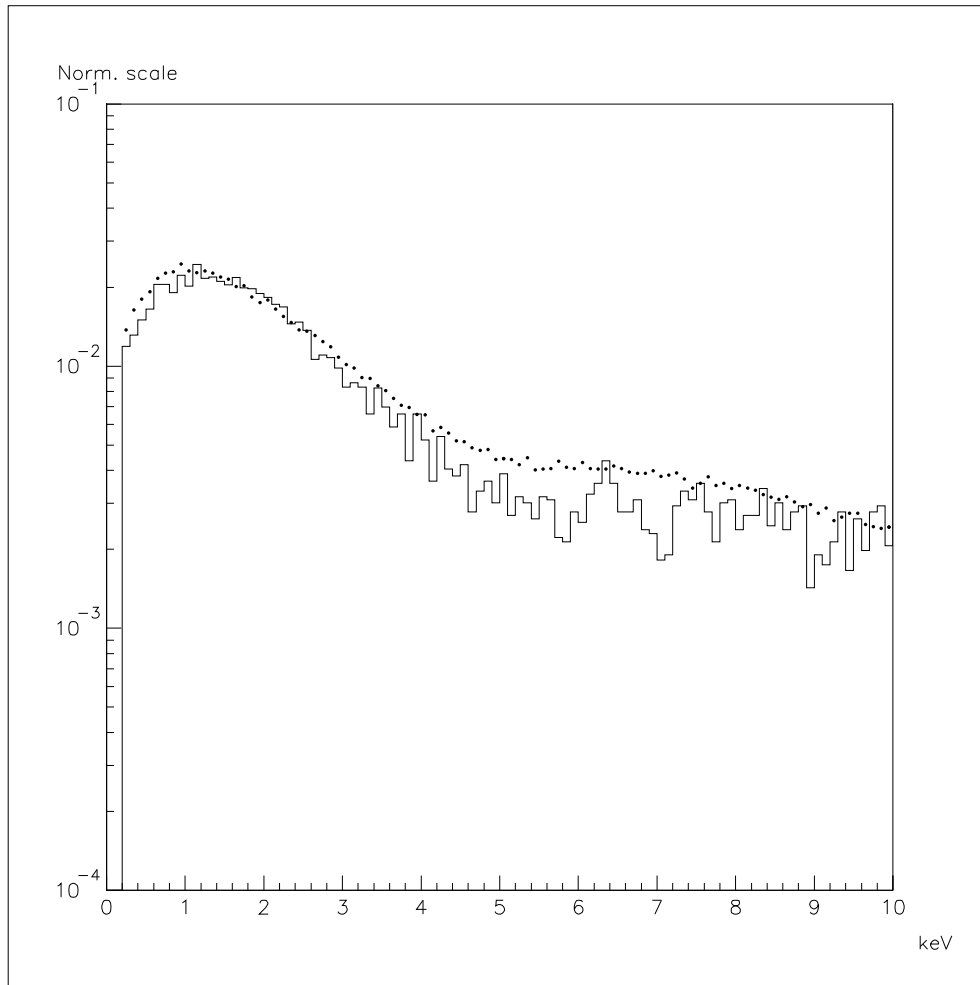


Figure 3.4: Energy spectrum of the hit straws (deposited energy larger than 200 eV) on the fitted track for 30 GeV electrons. The solid line represents simulated events using an irregularity of $\alpha_1 = \alpha_2 = 0.25$. The dots represent measured data from the prototype.

Chapter 4

Conclusions

The integrated transition radiation and tracking detector (TRT) is sensitive to the ionizations caused by the passing charged particles, as well as to the transition radiation (TR) photons produced when the particles pass through the radiator of the detector. In order to simulate the response of the detector to the charged particles the energy loss in the detector gas must be simulated.

The traditional way to implement the energy loss simulation is based on the Bethe Bloch formula with Landau fluctuations. This has been found to be inadequate in this case (see fig. 2.2). The reason for this is the small diameter of the straw proportional tubes in the detector prototype, which makes the number of energy transfers from the passing particles to the detector gas too few in each straw to allow the statistical fluctuations to be simulated in a satisfactory way by a model which is based on a continuous energy loss.

The photoadsorption ionization (PAI) model (described in chapter 2) on the other hand, treats the energy loss as a Poisson process for which the number of primary energy transfers from the particle to the detector gas can be simulated using a random generator. In this way the statistical fluctuations of the energy loss in the detector can be taken into account in a satisfactory manner (see fig. 2.1).

The model used for simulating the TR yield from relativistic particles passing radiators with different degrees of irregularity is described in chapter 3. As can be seen from fig. 3.2 the total TR yield is not affected significantly by small or moderate irregularities in the radiator, although the maxima caused by interference effects average out more and more as the radiator becomes more irregular. For large irregularities the yield starts to decrease.

The plastic foam to be used should be as regular as possible in order to maximize the TR yield. Therefore polyethylene is better suited for this purpose than e.g. polystyrene due to the more regular structure of this kind of plastic (see fig. 3.3).

Altogether these simulations reproduce the data from the prototype in a satisfactory way. The procedure described in this thesis is therefore suitable to be

used as a basis for the simulations of the TRT in the Inner Detector of the future ATLAS experiment.

Acknowledgements

First I would like to thank CERN for accepting me as a summer student during the summer of 1994. This has given me the opportunity to work at CERN for 13 weeks and it has been an interesting work, out of which eventually this thesis resulted.

I also would like to thank my supervisor at CERN, Dr. Wolfgang Funk, who despite the fact that he agreed to supervise my work on a very short notice did it excellently. He also put most of the simulation program together.

I would also like to give my thanks to the RD6 collaboration who initiated these simulation studies and without whose work there wouldn't have been any measurements to compare the simulations to.

I would also like to mention all the people I met at CERN: Christian Fabjan, Pavel Nevski, Sergey Konovalov and others, with whom I have had fruitful discussions regarding my work.

I would also like to thank my examiner, Tord Ekelöf from the Department of Radiation Sciences at Uppsala University, for his constructive remarks on the text and Robert Reineck at Uppsala University PET Centre for his assistance when printing out the colour pictures. These pictures were obtained from the ATLAS collaboration World Wide Web server (<http://atlasinfo.cern.ch>).

Bibliography

- [1] ATLAS collaboration, Technical Proposal for a General Purpose pp Experiment at the Large Hadron Collider at CERN, CERN/LHCC/94-43
- [2] RD6 collaboration, Particle Identification Performance of a Straw Transition Radiation Tracker Prototype, submitted to Nucl. Instrum. Methods
- [3] RD6 collaboration, Tracking Performance of a Straw Transition Radiation Tracker Prototype, submitted to Nucl. Instrum. Methods
- [4] ATLAS collaboration, The ATLAS Inner Detector, Status Report, CERN/LHCC/93-24
- [5] Detector R&D Proposal, Integrated High-rate Transition Radiation Detector and Tracking Chamber for the LHC, CERN/DRDC/90-38
- [6] Integrated Transition Radiation and Tracking Detector for LHC, RD6 status report, CERN/DRDC/91-47
- [7] Integrated Transition Radiation and Tracking Detector for LHC, RD6 status report, CERN/DRDC/93-46
- [8] RD6 collaboration, Systematic Study of Straw Proportional Tubes for the ATLAS Inner Detector, ATLAS Internal Note, INDET-No-18, submitted to Nucl. Instrum. Methods
- [9] GEANT, Detector Description and Simulation Tool, CERN Program Library Long Writeup W5013, Application Software Group, Computing and Networks Division, CERN
- [10] V. M. Grishin, V. K. Ermilova and S. K. Kotelnikov, Nucl. Instrum. Methods A307 (1991) 273
- [11] V. A. Chechin, L. P. Kotenko, G. I. Merson and V. C. Yermilova, Nucl. Instrum. Methods 98 (1972) 577
- [12] F. Lapique and F. Piuz, Nucl. Instrum. Methods 175 (1980) 297

- [13] V. Ginzburg and I. Frank, Zh. Eksp. Teor. Fiz. 16 (1946) 15 (in Russian), Journ. of Phys. 9 (1945) 353 (in English)
- [14] Michael L. Cherry, Gernot Hartmann, Dietrich Müller and Thomas A. Prince, Phys. Rev. D 10 (1974) 3594
- [15] G. M. Garibyan, L. A. Gevorgyan and C. Yang, Zh. Eksp. Teor. Fiz. 66 (1974) 552 (in Russian), Sov. Phys. JETP 39 (1974) 265 (in English)
- [16] G. M. Garibyan, L. A. Gevorgian and C. Yang, Nucl. Instrum. Methods 125 (1975) 133

In equation (5) in this reference the expression for Q should read

$$Q = \frac{1+p}{2}(1+h_a h_b) - h_a - p h_b$$

- [17] Boris Dolgoshein, Nucl. Instrum. Methods A326 (1993) 434